Molecular Dynamics Simulation of the Kinetics of Spontaneous Micelle Formation

S. J. Marrink*

Department of Biophysical Chemistry, University of Groningen, Nijenborgh 4, 9747 AG Groningen, The Netherlands

D. P. Tieleman

Laboratory of Molecular Biophysics, Rex Richards Building, University of Oxford, South Parks Road, Oxford OX1 3QU, U.K.

A. E. Mark

Department of Biophysical Chemistry, University of Groningen, Nijenborgh 4, 9747 AG Groningen, The Netherlands

Received: May 23, 2000; In Final Form: August 29, 2000

Using an atom based force field, molecular dynamics (MD) simulations of 54 dodecylphosphocholine (DPC) surfactant molecules in water at two different concentrations above the critical micelle concentration have been performed. Starting from a random distribution of surfactants, we observed the spontaneous aggregation of the surfactants into a single micelle. At the higher DPC concentration (0.46 M) the surfactants aggregated into a worm-like micelle within 1 ns, whereas at lower concentration (0.12 M) they aggregated on a slower time scale (∼12 ns) into a spherical micelle. The difference in the final aggregate is a direct consequence of the system achieving the lowest free energy configuration for a given quantity of surfactant within the periodic boundary conditions. The simulation at low surfactant concentration was repeated three times in order to obtain statistics on the rate of aggregation. It was found that the aggregation occurs at a (virtually) constant rate with a rate constant of $k = 1 \times 10^{-4}$ ps^{-1}. This is an unexpected result. On the basis of Monte Carlo simulations of a stochastic description of the system, using diffusion rates and cluster radii as determined by separate MD simulations of single DPC clusters, a lower rate constant which diminishes in the course of the aggregation process had been predicted. Neglect of hydrodynamic interactions, of long-range hydrophobic interactions, or of spatial correlations in the stochastic approach might account for the descrepancies with the more accurate MD simulations.

I. Introduction

Above their critical micellar concentration (cmc), surfactants aggregate spontaneously to form a wide variety of assemblies ranging from micelles, rodlike structures, and bilayers to more complex phases such as cubic phases. This self-aggregation process of surfactants is of fundamental importance to many biological and industrial processes. Although a lot of work, both experimentally and theoretically, is directed at an understanding of the various surfactant phases and the transitions between them, the actual initial process of self-aggregation has received little attention. This is primarily due to the fact that it occurs on a very fast time scale (nanosecond), and on a very short length scale (nanometer), thus making experimental investigation difficult.

Theoretically, self-assembly of model surfactants (consisting of a few beads only) was first studied in the early nineties by Smit et al.[1] for ternary water/oil/surfactant systems, using molecular dynamics (MD) simulations. They observed the spontaneous aggregation of simplified surfactants into either micelles inside a water-like environment, or reverse micelles in the oil-like environment. In a subsequent study[2] they were able to qualitatively reproduce the experimentally observed shape of the micellar size distribution. More recently, Lipowsky and co-workers[3] started systematic Monte Carlo (MC) studies of the self-aggregation of similarly simplified surfactants and deduced conditions for which micelles, rodlike micelles and bilayers are formed. Other simplified models that are currently used to study aggregation processes of surfactant(-like) molecules include lattice Brownian dynamics simulations[4] and MC simulations of the reaction probability density function.[5]

Until recently, more realistic modeling of self-aggregation using all-atom models has not been possible due to limitations in the required computer power. Hence, all atom MD simulations usually start with the surfactants in their target phase. After a suitable equilibration time during which the surfactants can relax into the phase of the system, various equilibrium properties of the system can be computed and compared to experimentally available data. Over the past decade or so it has been possible to obtain a detailed understanding of the behavior of surfactants in both bilayer[6] and micellar[7] phases.

Nowadays, due to the increase in computer power and due to algorithmic advances it is however possible to simulate the self-aggregation of surfactants using atomistic MD simulations. Salaniwal et al.[8] simulated the self-assembly of reverse micelles in water/surfactant/carbon-dioxide systems. They showed a rapid

* Corresponding author. E-mail: marrink@chem.rug.nl. Fax: 31503634800.

10.1021/jp001898h CCC: $19.00
Published on Web 12/02/2000

aggregation (within a nanosecond) of an initially dispersed system into a system containing three reversed micelles. Whether this constitutes the final equilibrium stage of the system remains unclear for the simulations were not continued. Maillet et al.[9] simulated the self-aggregation of both short and long chain ionic surfactants. They also observed fast aggregation on a nanosecond time scale, with two small micelles having formed (around 20 surfactants) in accordance with experimental predictions. Although no detailed analysis of the kinetics of aggregation is given, the authors conclude that the initial self-aggregation process is an off-equilibrium process which is dominated by collisions of clusters with different sizes, whereas the subsequent near equilibrium processes are dominated by single surfactant exchanges.

In this paper we aim to understand the kinetic processes that dominate the initial aggregation rate of surfactants in solution in more detail. We start our simulations from random initial structures and observe the spontaneous aggregation of surfactants into either spherical micelles or worm-like micelles depending on surfactant concentration. The kinetics of the aggregation process are analyzed in detail and compared to theoretically predicted aggregation rates. The surfactant chosen for this study was dodecylphosphocholine (DPC), a widely studied surfactant (mainly as a mimic for bilayer environments; see, e.g., refs 10 and 11) that forms small spherical micelles of an aggregation number of between 50 and 60 above a cmc of ~1 mM.[12] Recent MD simulations of DPC micelles have appeared in the literature,[13,14] offering a comparison between the structure of preassembled micelles and spontaneously aggregated ones obtained in this study.

The outline of the rest of this paper is as follows. First the relevant theoretical framework that describes the kinetics of aggregation is presented. In the subsequent section details of the simulation and analysis procedures are provided, followed by the results. A critical discussion of the results and their implications forms the last section.

II. Theory

The aggregation of surfactants into clusters of surfactants, and eventually into micelles, can be described, to first order, using the general framework of (ir-)reversible coagulation processes (i.e., refs 15 and 16). Within this framework, the reaction rate for the aggregation/disaggregation process of two clusters is given by

$$[\mathrm{M}_i] + [\mathrm{M}_j] \underset{k_{i,j}^{\mathrm{dis}}}{\overset{k_{i,j}^{\mathrm{agg}}}{\rightleftharpoons}} [\mathrm{M}_{i+j}] \tag{1}$$

where $[\mathrm{M}_n]$ is the concentration of clusters containg n surfactants and $k_{i,j}^{\mathrm{agg}}$, $k_{i,j}^{\mathrm{dis}}$ are the rate constants of aggregation and dissociation. If the dissociation rate is much slower than the association rate, we can neglect the dissociation process and the following rate equation can be derived for the aggregation process of smaller clusters into larger ones:

$$\mathrm{d}[\mathrm{M}_i]/\mathrm{d}t = \sum_{j=1}^{i/2} k_{i-j,j}[\mathrm{M}_{i-j}][\mathrm{M}_j] - [\mathrm{M}_i]\sum_{j=1} k_{i,j}[\mathrm{M}_j] - k_{i,i}[\mathrm{M}_i]^2 \tag{2}$$

with $k_{i,j} = k_{i,j}^{\mathrm{agg}}$. The positive term in eq 2 describes the formation of clusters of size i due to the merging of smaller ones, and the negative terms describe their disappearance due to collisions with other clusters. Note the double counting of collisions with $i = j$. In the limit of diffusion-controlled aggregation, the rate constant is given by

$$k_{ij} = 4\pi(D_i + D_j)(R_i + R_j) \tag{3}$$

where D_n is the diffusion constant of a cluster of n surfactants and R_n its collision radius. For uniform spheres, Stokes' law predicts $D \propto 1/R$ and the rate constant becomes only weakly dependent on particle size, the factor $(R_i + R_j)(R_i^{-1} + R_j^{-1})$ varying between 4 ($R_i = R_j$) and R_i/R_j ($R_i \gg R_j$). Assuming $k = k_{i,j}$, i.e., a size independent rate constant, eq 2 can be solved exactly. With the intial condition that there are only single surfactants at $t = 0$, the general solution to eq 2 reads

$$[\mathrm{M}_n](t) = [\mathrm{M}_1](0)\left(\frac{t}{\tau}\right)^{n-1}\left(1 + \frac{t}{\tau}\right)^{-n-1} \tag{4}$$

where $\tau = 2/k[M_1](0)$ is the characteristic time of aggregation. For the total number of clusters we have

$$[\mathrm{M}_{\mathrm{tot}}](t) = \sum_n [\mathrm{M}_n](t) = \frac{[\mathrm{M}_1](0)}{1 + t/\tau} \tag{5}$$

In the case of interacting particles, the expression for the rate constant k can be modified to include the interaction potential $V(r)$ of the particles:

$$k_{i,j} = 4\pi(D_i + D_j)/\int_{R_i+R_j}^{\infty} r^{-2} \mathrm{e}^{V(r)/kT}\,\mathrm{d}r \tag{6}$$

If the particles are strongly interacting ($V(r) \ll -kT$) once they approach each other to within a certain distance $r_c > R_i + R_j$, then $\mathrm{e}^{V(r)/kT} \rightarrow 0$ for $r > r_c$ and the integral of eq 6 can be replaced by

$$\int_{R_i+R_j}^{\infty} r^{-2} \mathrm{e}^{V(r)/kT}\,\mathrm{d}r \simeq \int_{r_c}^{\infty} r^{-2}\,\mathrm{d}r \tag{7}$$

resulting in

$$k_{i,j} = 4\pi(D_i + D_j)r_c \tag{8}$$

i.e., the effective collision radius is now determined by the range r_c of the strong interaction.

The above equations apply strictly in the thermodynamic limit only, when the volume approaches infinity and clusters are distributed homogeneously throughout the volume, neglecting the effect of correlations and fluctuations. Whether this limit applies to our system, which is finite containing a limited number of colliding molecules only, is not immediately clear. In addition, eq 2 can only be solved analytically for a size independent aggregation rate. We will therefore also use the stochastic approach as proposed by Gillespie[17] to predict the kinetics of aggregation in a finite system. Instead of solving the deterministic set of coupled differential equations in eq 2, the stochastic method replaces them by a single master equation describing the time evolution of the reaction probability density function $P(t_{\mathrm{dead}},\mu;t)$. It considers the time evolution of the system as a discrete chain of Markov events μ that happen in an infinitesimal time interval dt after an exponentially distributed dead time interval t_{dead} during which nothing happens:

$$P(t_{\mathrm{dead}},\mu;t)\,\mathrm{d}t = k_\mu^s\, h_\mu \mathrm{e}^{-\Sigma_\mu k_\mu^s h_\mu t_{\mathrm{dead}}} \tag{9}$$

In our case μ denotes one of the possible aggregation steps of cluster sizes i and j, $k_\mu^s = k_\mu/V$ is the stochastic rate constant for an aggregation taking place in a fixed volume V, and h_μ describes the combinatorial possibility for the aggregation step

μ. Considering only two clusters combining we have $h_\mu = M_i M_j$ for $i \neq j$ and $h_\mu = {}^1/_2 M_i(M_i - 1)$ for $i = j$, with M_i denoting the number of clusters present in V, i.e., $M_i = V\,[M_i]$.

Equation 9 can be solved with a Monte Carlo procedure.[17] Given an initial distribution of cluster sizes at $t = 0$, the procedure consists of generating a Markov chain of aggregation events. For each event two random numbers x_1 and x_2 in the unit interval are generated from which the next dead time t_{dead} and the specific aggregation step μ_i taking place can be determined according to the following equations:

$$t_{\text{dead}} = [\sum_{\mu} k_\mu^s h_\mu]^{-1} \ln(1/x_1) \tag{10}$$

and

$$\sum_{\mu}^{\mu_i - 1} k_\mu^s h_\mu < x_2 \sum_{\mu} k_\mu^s h_\mu \leq \sum_{\mu}^{\mu_i} k_\mu^s h_\mu \tag{11}$$

Repeating the procedure for a suitable number of events, the time evolution of the aggregation of surfactant clusters is generated. Averaging over a large number of different random number sequences provides both the average kinetics and the expected fluctuations in a finite system. The stochastic method has recently successfully been applied to study the kinetics of micellization away from the thermodynamic limit.[5]

III. Method

A. Simulation Details. We used the GROMACS package (v2.0)[18] for our MD simulations. Details of the DPC force field can be found in ref 14. The water was modeled as SPC.[19] The system was coupled to an isotropic pressure bath of 1 atm, and a heat bath of 300 K using standard coupling schemes.[20] Using the fast LINCS[21] and SETTLE[22] algorithms to constrain the bond lengths within the lipids and to constrain the water geometry, respectively, the use of a 5 fs time step was permitted.[23] A group based twin cutoff scheme was employed for the nonbonded interactions, with $R_{\text{cut}} = 1.0$ nm for Lennard-Jones and $R_{\text{cut}} = 1.5$ nm for electrostatic interactions.

Tieleman et al.[14] simulated, at similar conditions, three differently sized micelles of DPC containing 40, 54, and 65 surfactant molecules. Comparing energies and solvent accessible surface, they concluded that the most stable micelle size was likely to be at least 54, in accordance with experimental evidence based on quasi-elastic light scattering and analytical ultracentrifugation.[12] Therefore, we choose to simulate 54 DPC molecules, positioned at initial random positions in a cubic simulation box which was then filled with SPC water. The first system simulated contained the same number of waters as Tieleman's system,[14] i.e., 97 waters/surfactant equaling a surfactant concentration of 0.46 M. We will label this system "RANDOM54highA". As shown in the next section the periodicity of the system at this concentration favors the formation of a rod-like micelle rather than a spherical one. Identical results were obtained when repeated, starting from a different random distribution of surfactants throughout the box ("RANDOM54highB"). Therefore, the amount of water was increased by roughly a factor of 4 (416 waters/surfactant), implying a surfactant concentration of 0.12 M ("RANDOM54A"). In this case we observed the spontaneous aggregation into a single spherical micelle after 12 ns of simulation (see results section). The simulation was extended for another 6 ns to allow the micelle to relax toward its equilibrium structure. To increase the statistics of the initial aggregation process, this system was simulated three more times up to 6 ns with different initial random placement of the surfactant molecules. These three additional simulations are labeled "RANDOM54B .. RANDOM54D". Note that all systems have a concentration much higher than the cmc of DPC ($\sim$1 mM[12]). The simulations were performed in parallel on an IBM SP2 supercomputer, achieving a rate of $\sim$60 CPU hours/ns using 8 nodes.

TABLE 1: Overview of MD Simulations

label	# DPC	# SPC	⟨box edge⟩ (nm)	time (ns)
RANDOM54highA	54	5238	5.8	10
RANDOM54highB	54	5238	5.8	10
RANDOM54A	54	22496	9.0	18
RANDOM54B	54	22488	9.0	6
RANDOM54C	54	22484	9.0	6
RANDOM54D	54	22496	9.0	6
CLUS1	1	582	2.7	50
CLUS2	2	1507	3.6	50
CLUS3	3	1481	3.6	50
CLUS5	5	1438	3.6	50
CLUS10	10	2784	4.5	50
MICEL54	54	5238	5.8	14

To study some specific properties of smaller clusters, we also performed small scale simulations with clusters of one, two, three, five, and ten DPC molecules in excess SPC water (labeled CLUS1 ... CLUS10). Using the same simulation parameters as described above, 50 ns runs of these systems were performed, from which accurate data on cluster radius and diffusion rates could be obtained, as well as insight into the stability of small size clusters. All of these small scale simulations were performed on single processor Silicon Graphics O2 workstations. A full list of all the simulations we have performed, including details about the compositions and the total amount of simulation time, is given in Table 1. Also listed is the extended 14 ns simulation of the 54 DPC micelle of Tieleman[14] (labeled "MICEL54") on which some additional analysis was performed.

B. Analysis Details. To identify the formation of clusters of surfactants, we need a definition of what makes up a cluster. As two surfactant molecules have many different ways of interacting, any definition in terms of number of methyl−methyl contacts or headgroup-headgroup distance will be too specific. We therefore have used a general criterium based on the distance between the centers of mass of the surfactants. Two surfactant molecules are defined to be in the same cluster if the distance between their centers of mass, R_{com} is smaller than a certain cutoff distance which we call R_{agg}. On the basis of visual inspection of the CLUS2 trajectory (which shows occasions where the two surfactant molecules disaggregate) we find R_{agg} to be within the range 1.0 nm $< R_{\text{agg}} <$1.4 nm. A value of R_{agg} 1.2 nm was used for the analysis, but the results do not depend significantly on the precise choice of R_{agg} within the indicated range. For the stability of a cluster the following definition was used. If $R_{\text{com}} > R_{\text{agg}}$ for a period longer than 100 ps, the cluster is assumed to have fallen apart into two (or more) separate clusters.

To compare our aggregation rates to theoretically predicted ones, we need an estimate of both the effective radius of a cluster as well as its diffusion constant. Assuming that the clusters are on average spherically shaped, the effective radius R of the cluster is related to the radius of gyration R_{g} via

$$R = \sqrt{\left(\frac{5}{3}\right)} R_{\text{g}} \tag{12}$$

An accurate value for the average radius of gyration can be obtained from the 50 ns simulations of separate clusters. Using

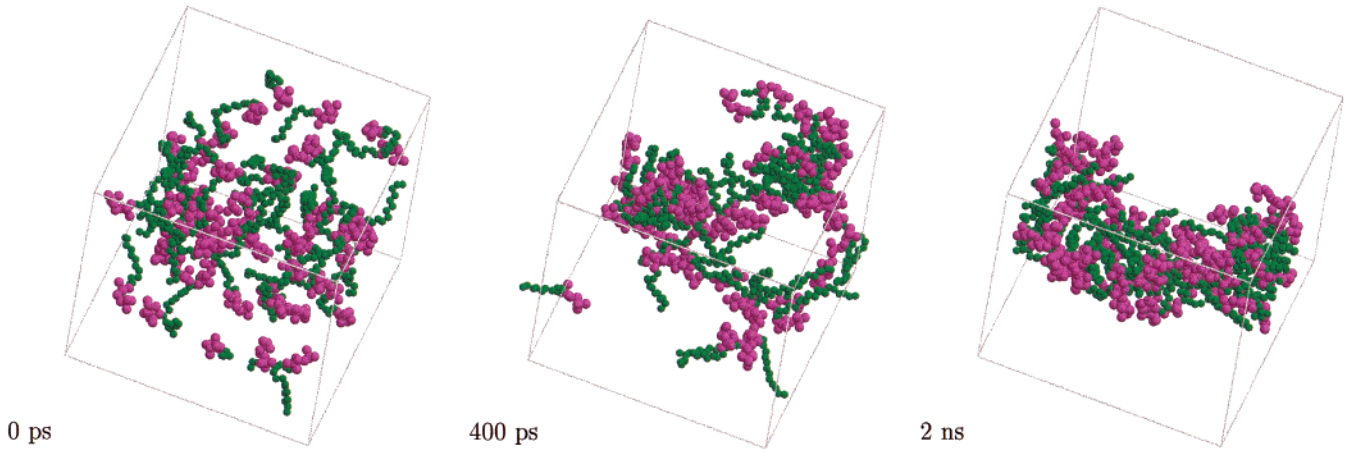

Figure 1. Spontaneous aggregation of DPC surfactants into a wormlike micelle at high concentration. Snapshots of the simulation at the start ($t = 0$ ps), intermediate ($t = 400$ ps), and micelle stage ($t = 2$ ns) are shown. DPC headgroups are drawn in purple, DPC tails in green. Water is ommitted for clarity.

a similar definition of micelle radius, Bogusz et al.[24] obtained agreement between their MD simulations and the experimentally determined radius for glucoside micelles. Note that this definition of a micelle radius is only approximate, as the micelles are not perfect spheres but rather ellipsoidal, both at low and at high aggregation numbers.[24] The diffusion constant is estimated from the mean square displacement (MSD) of the center of mass of the cluster. Because of internal motion within the cluster plus momentum effects, the MSD displays both a short time regime with an apparent diffusion rate D_{short} which is somewhat higher than the limiting diffusion rate D_{long} of the cluster itself. We find that for times beyond ~200 ps the internal motion of the small clusters is averaged sufficiently and does not contribute significantly to the long time diffusion constant. For the entire 54 surfactant micelle the internal motions take much longer to average out (>1 ns). Our statistics in this case are not accurate enough to make the distinction between these two regimes.

IV. Results

A. Aggregation into a Worm-Like Micelle. Figure 1 illustrates the spontaneous aggregation process for 54 DPC surfactants at high concentration (0.46 M). At this high concentration the aggregation takes place very rapidly, with a rodlike micelle formed within 1 ns. The rodlike micelle remains stable during the remainder of the simulation (10 ns), although it takes over 5 ns for the rodlike micelle to relax into its final structure. The same qualitative picture emerged when we repeated the simulation starting from different random surfactant positions: again a stable periodic rodlike micelle was formed within 1 ns. If we assume that the main driving force to form aggregates is a reduction of the exposed hydrocarbon area, and that DPC has a bulky headgroup with respect to its hydrocarbon tail, then one would expect spherically shaped aggregates to be energetically more favorable as they have the smallest area compared to volume. However the use of periodic boundary conditions means it is possible to form periodic aggregates as a way of avoiding the creation of an additional interface thus increasing the ratio of volume to surface area. Given the surface area A_{sphere} and radius R_{sphere} of a spherical micelle, it is straightforward to compute the expected relative increase in surface area A_{cyl} and radius R_{cyl} of a periodic cylindrical micelle with the same volume. Given the length of the simulation box L, we have $A_{\text{cyl}}/A_{\text{sphere}} = \sqrt{L/3R_{sphere}}$ and $R_{\text{cyl}}/R_{\text{sphere}} = \sqrt{4R_{\text{sphere}}/3L}$.

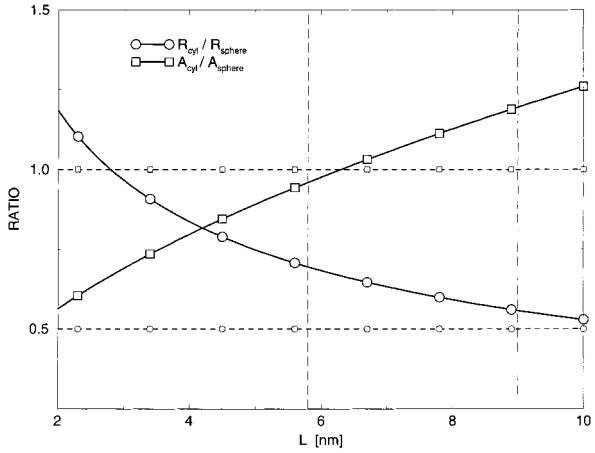

Figure 2. Stabilization range of periodic-cylindrically vs spherically shaped micelles. The solid curve represents the ratio of the radius (circles) and surface area (squares) of a periodic-cylindrically vs spherically shaped micelle for a given box length, using $R_{\text{sphere}} = 2.1$ nm (estimated using eq 12 and $R_g = 1.6$ nm[14]). The horizontal dashed lines represent the limits of expected stability for a periodic-cylindrical micelle; i.e., it cannot have a radius smaller than half that of a spherical micelle (at which radius the surfactants are fully interdigitated), and its surface area should be smaller than that of a spherical micelle. The vertical lines denote the box sizes of the simulated system, i.e., the small system at 5.8 nm producing a periodic-cylindrically shaped micelle, and the large system at 9.0 nm producing a spherically shaped micelle.

In Figure 2 is plotted the expected stabilization range of a periodic cylindrically shaped micelle *vs* a spherically shaped one based on the above expressions for the ratios of surface area and micelle radius. It can be seen that up to box lengths of approximately 6 nm the area of a periodic cylindrical micelle is actually smaller than that of a spherical one. However, there is another limit to the stabilization of a cylindrical micelle, namely that its radius cannot be smaller than half that of a spherical micelle, which would require more than fully interdigitated surfactants. This limit is reached much further away, above 10 nm. Given the box length that we used in our first simulation, i.e., 5.8 nm, one would indeed expect the periodic cylindrical micelle to be most stable, in accordance with our findings. Also, inspection of Figure 1 reveals that the surfactants are to a large extent interdigitated, in agreement with the predictions of Figure 2 which indicate a cylinderal micelle radius of ≃70% of that of a spherical micelle.

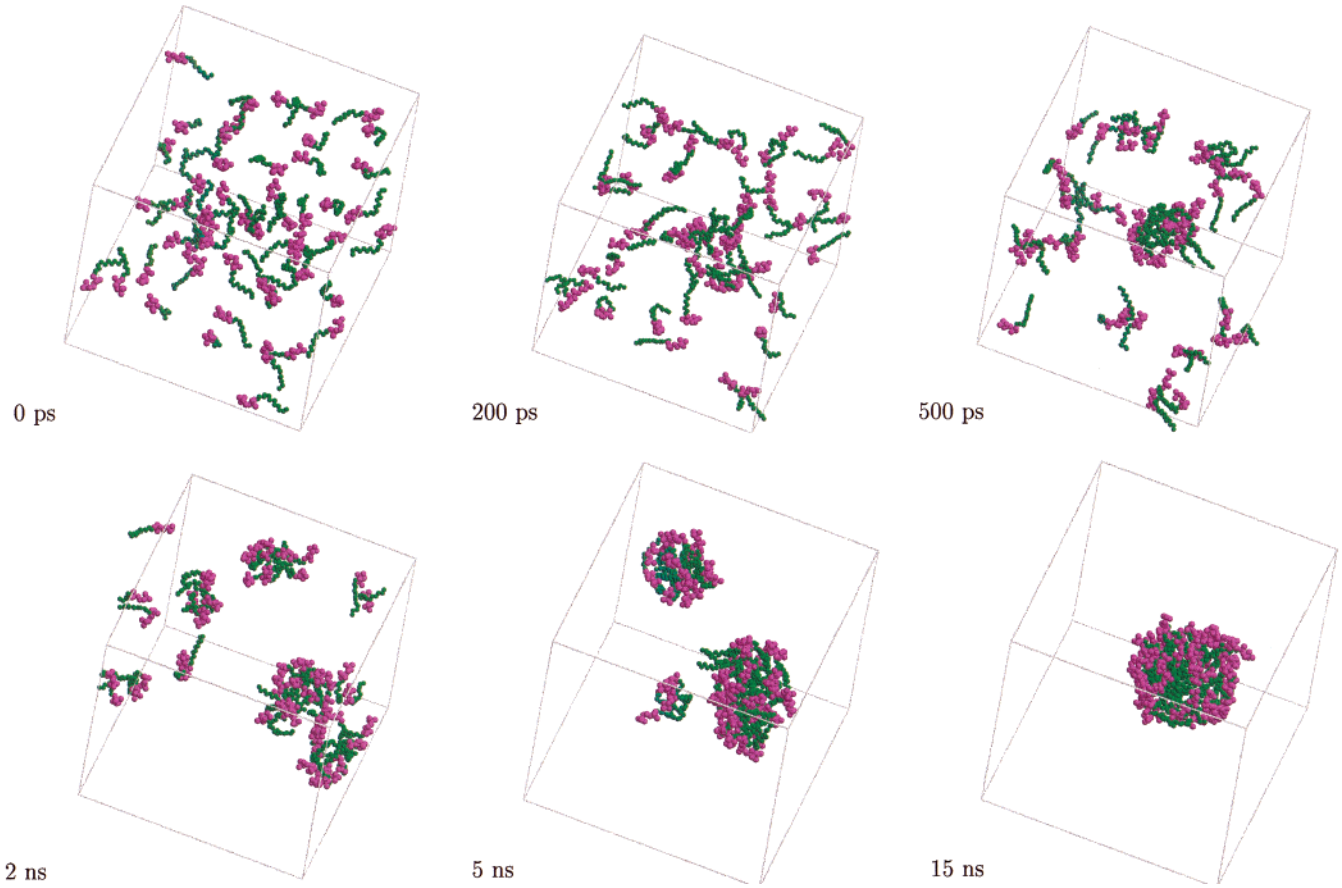

Figure 3. Spontaneous aggregation of DPC surfactants into a spherical micelle at low concentration. Snapshots of the simulation at the start ($t = 0$ ps), intermediate ($t = 200$ ps, 500 ps, 2 ns, 5 ns), and micellar stage ($t = 15$ ns) are shown. DPC headgroups are drawn in purple, DPC tails in green. Water is ommitted for clarity.

B. Aggregation into a Spherical Micelle. To get rid of the artificial effect of the periodic boundary conditions, it is clear that we need to simulate a larger system. From the surface ratio as shown in Figure 2 we deduced that with an increase of the box size to 9.0 nm the spherical micelle should be the preferred phase over a periodic rodlike structure. We therefore simulated the aggregation process for 54 DPC surfactants at this increased system size (RANDOM54A), implying an approximately 4-fold lower concentration of surfactants (0.12 M). In Figure 3 we show that now indeed a spherical micelle is being formed, rather than a cylindrical one. The final single micelle first appears after ~12 ns. It takes another 5 ns for the micelle to reach its equilibrium structure. (Where one merely aims to obtain an unbiased starting structure, one can accelerate the aggregation rate by draining the system as soon as the number of separate clusters has dropped considerably. In a separate simulation (results not shown) one-third of the number of water molecules were removed randomly after the system had aggregated into four separate clusters, and once more after only two clusters remained. Thus, we obtained a single spherical micelle within 6 ns simulation, as opposed to the ~12 ns of the normal simulation.)

It is interesting to compare the equilibrium structure of the finally obtained micelle to the equilibrium structure of the preassembled one (MICEL54) that was simulated by Tieleman et al.[14] It is found that the radial distribution of atoms, the solvent accessible surface, the average radius of gyration and the ratio of the principal axes are indistinguisable within the observed fluctuations.

The simulation at low concentration was repeated three times (RANDOM54B .. RANDOM54D) for a duration of 6 ns, starting from different initial random placements of the surfactant, to provide improved statistics. In Figure 4 we display the decline of the total number of clusters during the simulation. Although the four different simulations show some scatter, the general aggregation process seems to be very similar—a fast initial clustering halving the total number of clusters in about 300 ps, followed by a much slower merging of the remaining clusters to form either 3 or 4 small micelles after 6 ns in all cases. In the extended simulation RANDOM54A two of the remaining three micelles merge after ~8.4 ns, and the remaining two micelles merge into the final micelle at $t = 11.9$ ns.

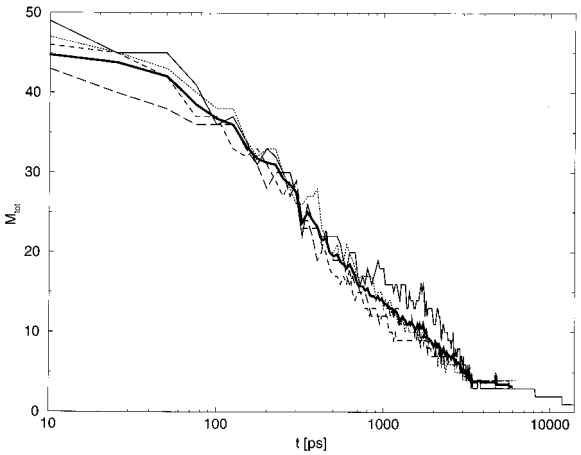

Figure 4. Reduction of total number of clusters with time for simulations RANDOM54A .. RANDOM54D. Separate thin lines indicate different simulations. The thick solid line denotes the average of the four simulations (up to 6 ns).

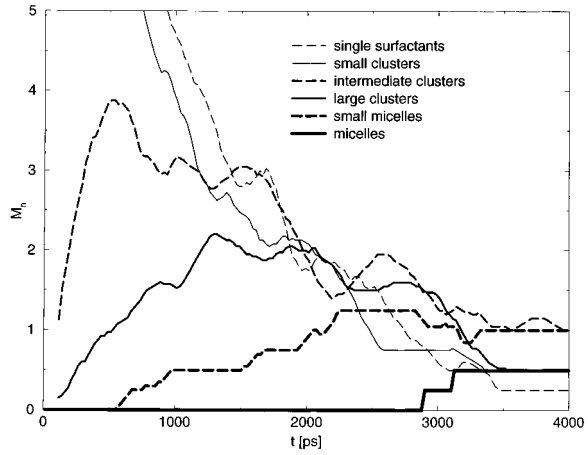

Figure 5. Appearance and disappearance of clusters of various sizes during simulations RANDOM54A .. RANDOM54D. Graphs show average results of the four simulations, for six different cluster sizes: single surfactants, small clusters (between 2 and 4 surfactants), intermediate clusters (5−8), large clusters (9−15), small micelles (16−31), and micelles (32 or more surfactants).

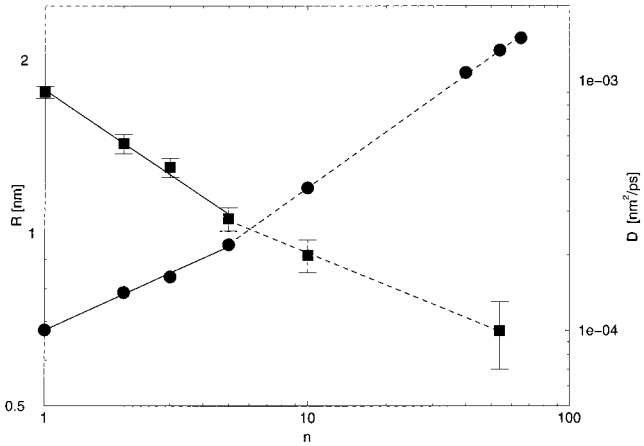

Figure 6. Radius and diffusion constants of surfactant clusters as a function of the number of surfactants. Circles (R) and squares (D) are results obtained from the simulations of isolated clusters (CLUS1 .. CLUS10) or taken from the simulation of Tieleman et al.[14] for $n = 40$, 54, and 65. Lines are linear fits on a log−log scale, in the range $n \leq 5$ (solid) and $n \geq 5$ (dashed). The error bars in the case of R are smaller than the symbols.

In Figure 5 we have plotted the separate time evolution of the emergence and disappearance of clusters of different aggregation numbers, averaged over the four simulations. We distinguish between six different classes of clusters: single surfactants, small clusters (2−4 surfactants), intermediate clusters (5−8), large clusters (9−16), small micelles (17−31) and micelles (≥32 surfactants). Apart from the single surfactant clusters and the micelle, all other cluster sizes display a maximum as they are first formed by the merging of smaller clusters and then disappear again when they aggregate into bigger ones. The shape of the curves is in qualitative agreement with those predicted by standard aggregation theory (eq 4).

C. Scaling of Cluster Properties. Before we can make a comparison of the simulated kinetics of aggregation with the theoretical predicted ones, we need to have an estimate of both the effective radii and diffusion rates of the individual clusters. Figure 6 plots these data for various cluster sizes as obtained from separate MD simulations of isolated clusters (CLUS1 ... CLUS10). The data for the largest cluster sizes is taken from the simulations of Tieleman et al.[14] The diffusion constants are based on a linear fit of the MSD curves up to 2 ns.

Both the radius and the diffusion constant clearly show two different scaling regimes. For clusters larger than 5 surfactants, the scaling is identical (within errorbars) to the scaling laws predicted for hard spheres: the radius scales with the number of surfactants n as $R \propto n^{0.33\pm0.01}$ and the diffusion constant scales as $D \propto n^{-0.4\pm0.1}$ (for hard spheres the scaling is given by $R \propto n^{1/3}$, $D \propto n^{-1/3}$). The same scaling for R was also observed in the simulations of octyl glucoside micelles for clusters between 10 and 75 surfactants.[24] The estimate of the long time diffusion constant that we obtain for the micelle of 54 DPC's ($10 \pm 4 \times 10^{-5}$ nm^2/ps) compares well to the experimentally determined values of 9.2×10^{-5} nm^2/ps (analytical ultracentrifugation[12]), 7.8×10^{-5} nm^2/ps (quasi-elastic lightscattering[12]), 9.2×10^{-5} nm^2/ps (NMR[10]). One has to bear in mind that the apparent close agreement might be somewhat fortuitous though. The experimentally obtained values are based on a micelle size distribution rather than on a single micelle size. Furthermore, concentration effects can play a role. Finally the SPC model for water is known to underestimate the viscosity of real water by roughly a factor of 2.

Not surprisingly the smallest clusters ($n \leq 5$) behave differently: the radius scales with a slightly smaller exponent, $R \propto n^{0.21\pm0.01}$ whereas the diffusion constant scales with a much larger one, $D \propto n^{-0.7\pm0.1}$. Analysis of the length of the principal axes of the clusters underlines the difference between small and larger clusters. Whereas clusters of 10 surfactants and larger are essentially spherical (with an average ratio between longest and smallest axis dropping from 1.4 for $n = 10$ to 1.1 for $n = 54$), the smallest clusters are shaped more irregularly. For these clusters their longest radius remains approximately constant (at 1.1 nm) whereas the two shorter axes stepwise increase upon addition of another surfactant. These data and visual inspection of these small clusters reveal that they form microscopic, fully interdigitated bilayers, with the longest radius approximately equaling half the length of a DPC surfactant. Nonspherical objects experience a higher friction which qualititatively explains the steeper dependency of diffusion rate on aggregation number. Using shape corrections on the friction coefficient for ellipsoidally shaped objects however we cannot account for the observed deviation from Stokesian behavior. With axis ratios between 2 and 3 as obtained from our simulations the predicted increase in friction is of the order of 5−10% only.

Bogusz et al.[24] find that clusters of 5 octyl glucoside are not stable beyond the nanosecond time scale, whereas clusters larger than 10 surfactants remain stable over a simulation time of 4 ns. We find that all clusters of DPC surfactants are fully stable during the 50 ns runs (CLUS2 .. CLUS10), except for the dimer which dissociated twice. Apparently the interaction between DPC surfactants is stronger than between octyl glucosides, probably due to the longer tail of DPC (12 methyl groups) compared to octyl glucosides (8 methyl groups). Short time escapes (shorter than 100 ps) of single surfactants occur more frequently, on average once per 5 ns, without a clear cluster size dependency. In any case the rate constant for the disaggregation process, k^{dis}, is much smaller than the rate constant k^{agg} of aggregation, making the assumption of an irreversible aggregation process on which eq 2 is based valid.

Given the diffusion constant D_i and the radius R_i of a cluster i, the rate constant $k_{i,j}$ of aggregation with another cluster j is given by eq 3. Using the scaling behavior of the diffusion constant and cluster radius with the number of surfactants as apparent from the single cluster simulations (i.e., Figure 6), the aggregation rate constants for any pair of clusters can be predicted. In the left panel of Figure 7 rate constants based on

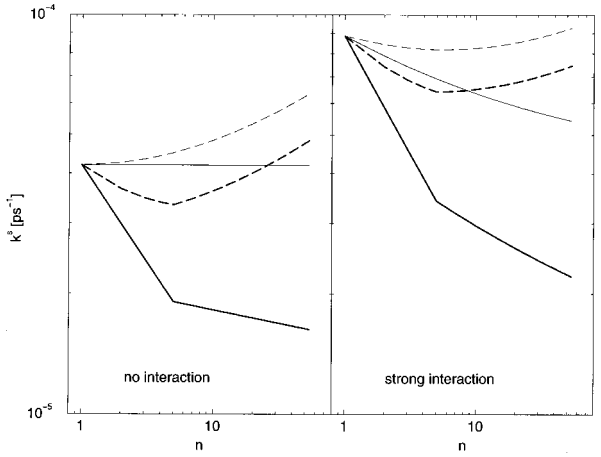

Figure 7. Comparison of stochastic rate constants k^s based on simulation data from Figure 6 and predictions for hard spheres. The left set of curves is computed using eq 3, i.e., assuming no interaction between the clusters, the right set of curves using eq 8 with $r_c = R_i + R_j + 1.5$ nm, i.e., the maximum possible direct attractive interaction. The thick lines are obtained from the fits to the simulation data in fiugre 6; the thin lines represent the hard sphere predictions. Solid lines denote $k_{i,j}$ with $i = j = n$, dashed lines with $i = 1$, $j = n$.

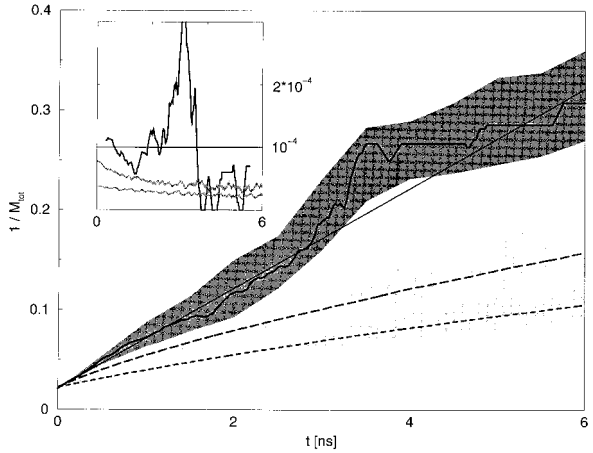

Figure 8. Simulated rate of cluster aggregation compared to theoretical predictions. The bold solid line is the rate of total cluster number reduction averaged over the four simulations RANDOM54A .. RANDOM54D. The thin solid line is a linear fit to these data. Two theoretical lines are shown according to eq 9 with collision rates based on simulation data as displayed in Figure 7. Dashed lines have no additional interaction, dotted lines have strong interaction over the maximum possible distance $r_c = R_i + R_j + 1.5$ nm. Gray area's denote the width of one standard deviation as obtained from different realizations. The inset shows the effective stochastic collision rate, obtained from the derivative of the curves (multiplied by 2) in units of ps^{-1}.

eq 3 (expressed as their stochastic value, $k^s = k/V$) are shown for pairs of equal size ($i = j$) and for pairs with one cluster having the maximum size, i.e., the complete micelle ($i = 54$). The same rate constants are shown based on the predictions for hard spheres ($R \propto n^{1/3}$, $D \propto 1/R$). In the case of hard spheres, the rate constants for aggregation of equally sized particles is constant, whereas the hetero aggregation rates are only weakly dependent on the difference in cluster number. The maximum ratio observed in the hard sphere approximation is $k_{1,54}/k_{54,54} \simeq 1.5$. Note that the absolute values of the rate constants based on hard spheres depend on the reference cluster size (here taken as $n = 1$) but their ratios do not. Clearly, the predictions for hard spheres are very different from the predictions based on the simulation data for single clusters, which have a much larger cluster size dependence especially in the range of the smallest clusters, with maximum ratios of $k_{1,1}/k_{54,54} \simeq 2.5$ for homo aggregation (i.e., between equally sized clusters), and $k_{1,54}/k_{54,54} \simeq 3$ for hetero aggregation (between clusters of different sizes). In the right panel of Figure 7 the same data are shown, but now with the assumption that a strong attractive force exist between the clusters that accelerates the aggregation. It was assumed that as soon as two surfactants are within their mutual cutoff distance as employed in the simulation i.e., $R_{cut} = 1.5$ nm, the clusters are strongly interacting ($V(r) \ll -kT$) and the rate constants are given by eq 8 instead of eq 3, with $r_c = R_i + R_j + 1.5$ nm. Comparing the aggregation rate constants with interaction to the ones without, it becomes apparent that the effect is strongest for the collision rate between the smallest clusters, which increase by a factor of more than 2. As the cutoff distance becomes smaller compared to the cluster radius, the effect becomes weaker, dropping to about a factor of 1.5 for the larger clusters.

D. Comparison to Kinetic Theory. In this section we will compare the rate of aggregation of DPC surfactants into a single spherical micelle as observed in the MD simulations to three levels of theoretical predictions. The simplest level is the analytical prediction of eq 5 which states that the total number of clusters diminishes in time with a constant rate constant. This prediction is based on the assumption that surfactant clusters essentially behave as hard spheres, and further that finite size effects can be neglected. The second level is based on a MC simulation of the stochastic eq 9, using the rate constants of Figure 7. This level is expected to be more accurate as it uses variable rate constants which are based on the diffusion constants and cluster radii of simulated clusters rather than hard spheres. Besides, it also takes into account the fact that the system is finite. The third level is a modification of the second level to include the effect of attractive interactions between the clusters through the use of the modified rate constants (right panel of Figure 7).

In Figure 8 we compare the average rate of aggregation obtained from the four simulations (RANDOM54A − D) to the theoretical predictions of the second and third level. The total number of cluster sizes M_{tot} is plotted inversely against time. Thus, the slope of the curve reflects the effective aggregation rate constant at any time. For the simplest level of theory a constant slope is predicted. In qualitative agreement with this level, the simulated data appear (up to ~3 ns) as a straight line, with a (virtually) time independent collision rate $k^s \simeq 1 \times 10^{-4}$ ps^{-1}. Given the results of Figure 7, this is unexpected. Indeed the rates predicted by the stochastic approach reflect a decrease in the apparent rate constant in a manner similar to the decrease of the pair collision rates of Figure 7. Therefore, the MD results and the stochastic results differ significantly. This is apart from the slope of the curves for $t >$ 3.5 ns from which it is however difficult to draw conclusions due to the poor statistics of the MD data. The initial slope of the MD data does compare reasonably well to the stochastic data assuming a strong aggregating driving force, but in the range 1 ns $< t <$ 3 ns the observed rate of aggregation is much higher than predicted by the stochastic approach, by at least a factor of 2. Inspection of Figure 5 reveals that during this time interval the aggregation of intermediate clusters into large clusters and small micelles is the dominant recombination step.

V. Discussion

The results of our simulations show that the spontaneous aggregation of DPC surfactants is much faster than can be

expected based on theoretical models, even if realistic (i.e., simulated) scaling of cluster radius and diffusion constant are taken into account. We now discuss some of the possible reasons for this discrepancy.

The presence of long range interactions could significantly enhance the aggregation rate. We tried to capture this effect in the stochastic modeling by using an effective collision radius (eq 8) based on the interaction cutoff of 1.5 nm as used in the simulations. This procedure considers two particles to be aggregated as soon as the distance between their surfaces lies within the interaction range set by the cutoff distance, thus mimicking the effect of an (infinitely) strong driving force. Although the resulting predicted increase in aggregation rate is large (roughly by a factor of 1.5; see Figure 8), it is not enough to account for the simulated rate of aggregation. Moreover, the decrease in aggregation rate constant for collisions between larger clusters remains, whereas a constant (or even increasing) rate constant is observed in the MD simulations. To bring the simulated and stochastic rates of aggregation into agreement, one would need even longer range interactions which would scale with cluster size. To test the hypothesis of a significant effect of long-range forces, we resimulated the first 3 ns of system RANDOM54A with a much shorter cutoff length (1.0 nm). As we did not see a significantly different aggregation behavior, we conclude that the presence of direct long range attractive forces is not likely to be the origin of the very fast aggregation. A water mediated hydrophobic attractive force could possibly offer an explanation.

One of the assumptions underlying eq 3 is that the collision between two particles is diffusion-controlled. To test whether this is the case in our system, we made a comparison between the decay time t_v of the velocity autocorrelation function (VACF) and the average dead time t_{dead} between collisions which is given by $t_{dead} = \{dM_{tot}/dt\}^{-1}$. With an almost constant rate constant as observed in the MD simulations, eq 5 can be used to obtain the analytic expression $t_{dead} = \tau/M_1(1 + t/\tau)^2$. The apparent collision rate $k^s \simeq 1 \times 10^{-4}$ ps^{-1} implies a characteristic time of aggregation of $\tau = 2/(k^s M_1) \simeq 350$ ps. This is the time in which the total number of clusters is halved (compare Figure 4). For $t < \tau$ the dead time is almost constant, with a value of $t_{dead} \simeq 10$ ps. For $t > \tau$ the dead time increases rapidly, $\propto t^2$. At $t = 3$ ns, the time where the simulated rate constant and the predicted one differ most, $t_{dead} \simeq 500$ ps. From the simulations CLUS1 and CLUS2−CLUS10 we computed the VACF of the center of mass, showing a decay time of around $t_v \simeq 1$ ps for the single surfactant, and 10 ps $< t_v <$ 25 ps for the clusters. The decay time of the VACF for the clusters is comparable to the initial dead time, which shows that during the initial stages of aggregation the diffusion-limited approximation is inappropriate. The short time aggregation rate using eq 3 will therefore be underestimated. To quantify this effect, an effective short time diffusion constant can be calculated from the slope of the mean squared displacement curves at short times. Fits up to 100 ps yield diffusion constants for small cluster that are between 25% and 50% higher. Using these effective short time diffusion constants, the initial differences between the simulated aggregation rate and the stochastic one (based on an effective collision radius) disappear. Compared to the dead time of 500 ps estimated for intermediate times, the decay times of the VACF of the simulated clusters become small. Therefore, the diffusion-limited aggregation regime is expected to be applicable, unless hydrodynamic effects are important. Hydrodynamic effects could increase the diffusion speed in the large systems while being absent in the small scale simulations of single clusters on which the estimate of the diffusion constants is based. This we leave for future investigations.

Another assumption underlying both the deterministic formulation (eq 2) and the stochastic approach (eq 9) is the spatial homogeneity of the system. This can only be achieved for systems where the collision rate is small compared to the diffusion rate, i.e., when the system has enough time between collisions to randomize the distribution of particles. This is clearly not the case in our system, even around the "critical" 2 ns time: During the estimated dead time interval of 300 ps, a typical cluster of 10 surfactants has a root-mean-square displacement of 0.6 nm only. Compared to the linear system size of 9.0 nm this is far too small to be able to homogeneize the system. Therefore, it seems reasonable to assume that the distribution of surfactants in our system remains correlated instead of homogeneous. For a nonuniform system one would expect a higher collision rate, possibly explaining the difference between the MD simulations and the stochastic approach. A more quantitative estimate of the effect of spatial correlations in cluster concentrations is hard to make, however.

Finally, two other possible factors that could contribute to a larger aggregation rate in the MD simulations in comparison with the stochastic predictions are the asphericity of the clusters and excluded volume effects. Self-evidently, the treatment of small clusters as spherical objects with a definite radius is an oversimplification. Although shape corrections based on an average ellipsoidal structure as observed in the single cluster simulations are rather small even for the smallest clusters, the clusters that form during the simulation need a considerable time to relax toward their equilibrium structure (around 200 ps for a cluster of 10 surfactants, around 5 ns for a 54 DPC micelle) which makes the asphericity of the clusters during the aggregation process possibly significantly larger. Consider the limiting possible effect of asphericity, i.e., that all the clusters are one surfactant thick cylinders with an effective collision radius which is an averaged value of the radius (equal to one surfactant) and length (scaling linearly with n, the number of surfactants) of the cylinder. Using this scaling relation for the collision radius (i.e., $R \propto (2 + n)/3$), the stochastic results come close to the simulated results. However, this scaling law is very exaggerated. For instance, it assumes a length of more than 10 nm for a cluster consisting of 10 surfactants. More realistic approaches fail to bridge the gap. The effect of excluded volume becomes nonnegligible for the larger clusters. For instance, for a cluster of 10 surfactants the excluded volume with respect to equally sized clusters is $\sim$58 nm^3 which is 8% of the total volume, and for a 54 DPC micelle with respect to a single surfactant it is $\sim$90 nm^3 or 12% of the total volume. The effective concentrations of the cluster becomes equally larger, and the collision rates which take into account exluded volume effects can therefore be expected in the above cases to be 8% and 12% higher than the collision rate without this effect. Although significant, this effect is also too small.

In future work we will hopefully be able to obtain more insight into the physical origin of the fast aggregation process. There is a need to study different concentrations and different surfactants, to determine whether the kinetics of micellization as observed in this work are universal or constitute a special case. Considering the observation of subnanosecond aggregation of such diverse systems as reversed micelles in carbon-dioxide[8] and of cationic micelles[9] in water, fast kinetics are likely to be universal. One would also like to simulate larger systems, where more than one final micelle can be formed, to obtain an equilibrium micellar size distribution which could be compared

to experimental values. The kinetics of micelle reorganizations around the equilibrium distribution are likely to be different (much slower) from the initial aggregation, as thermodynamic gradients are becoming much smaller. We are currently undertaking simulations of a system twice as large in each dimension, at the same surfactant concentration as the current system. Simulations of simplified models like the ones used by Smit[2] and Lipowsky[3] can further help to understand the descrepancy between the atomistic approach on one hand, and the theoretical descriptions on the other.

VI. Conclusion

We have shown the spontaneous aggregation of DPC surfactants in water into a spherical micelle using all atom MD simulations. The aggregation rate is much faster than expected on the basis of stochastic modeling, especially the rate of aggregation of clusters consisting roughly of between 5 and 15 surfactants. The total aggregation process for a system consisting of 54 DPC surfactant molecules and more than 20000 waters is found to be of the order of 12 ns, with a rate constant of $k \simeq 1 \times 10^{-4}$ ps^{-1} and a characteristic time of aggregation of $\sim$350 ps. At higher DPC concentrations, a worm-like micelle appears more stable than a spherical one, which can be explained in terms of exposed surface area.

Acknowledgment. D.P.T. acknowledges the European Molecular Biology Organization (EMBO) for a long-term fellowship.

References and Notes

(1) Smit, B.; Hilbers, P.; Esselink, K.; Rupert, L.; van Os, N.; Schlijper, A. *J. Phys. Chem.* **1991**, *95*, 6361.

(2) Smit, B.; Esselink, K.; Hilbers, P.; van Os, N.; Rupert, L.; Szleifer, I. *Langmuir* **1993**, *9*, 9.

(3) Goetz, R.; Lipowsky, R. *J. Chem. Phys.* **1998**, *108*, 7397.

(4) Lannibois, H.; Hasmy, A.; Botet, R.; Chariol, O.; Cabane, B. *J. Phys. II Fr.* **1997**, *7*, 319.

(5) Mavelli, F.; Maestro, M. *J. Chem. Phys.* **1999**, *111*, 4310.

(6) Tieleman, D. P.; Marrink, S. J.; Berendsen, H. J. C. *Biochim. Biophys. Acta* **1997**, *1331*, 235.

(7) Tarek, M.; Bandyopadhyay, S.; Klein, M. L. *J. Mol. Liq.* **1998**, *78*, 1.

(8) Salaniwal, S.; Cui, S.; Cummings, P.; Cochran, H. *Langmuir* **1999**, *15*, 5188.

(9) Maillet, J.; Lachet, V.; Coveney, V. *Phys. Chem. Chem. Phys.* **1999**, *1*, 5277.

(10) Kallick, D. A.; Tessmer, M. R.; Watts, C. R.; Li, C.-Y. *J. Magn. Reson. B* **1995**, *109*, 60.

(11) Beswick, V.; Guerois, R.; Cordier-Ochsenbein, F.; Coïc, Y.-M.; Huynh-Dinh, T.; Tostain, J.; Noël, J.-P.; Sanson, A.; Neumann, J.-M. *Eur. Biophys. J* **1998**, *28*, 48.

(12) Lauterwein, J.; Bösch, C.; Brown, L. R.; Wüthrich, K. *Biochim. Biophys. Acta* **1979**, *556*, 244.

(13) Wymore, T.; Gao, X. F.; Wong, T. C. *J. Mol. Struct.* **1999**, *195*, 485−*486*.

(14) Tieleman, D. P.; van der Spoel, D.; Berendsen, H. J. C. *J. Phys. Chem. B*, in press.

(15) Ginnel, R. *Association Theory*; Elsevier: Amsterdam, 1979.

(16) Evans, D.; Wennerstrom, H. *The Colloidal Domain: Where Physics, Chemistry, Biology, and Technology Meet*; Wiley: New York, 1999.

(17) Gillespie, D. *J. Comput. Phys.* **1976**, *22*, 403.

(18) van der Spoel, D.; van Buuren, A. R.; Apol, E.; Meulenhoff, P. J.; Tieleman, D. P.; Sijbers, A. L. T. M.; van Drunen, R.; Berendsen, H. J. C. *Gromacs User Manual version 1.2*, Nijenborgh 4, 9747 AG Groningen, The Netherlands. Internet: http://rugmd0.chem.rug.nl/ gmx, 1996.

(19) Berendsen, H. J. C.; Postma, J. P. M.; Gunsteren, W. F.; Hermans, J. Interaction models for water in relation to protein hydration. In *Intermolecular Forces*; Pullman, B., Ed.; Reidel: Dordrecht, The Netherlands, 1981; pp 331−342.

(20) Berendsen, H. J. C.; Postma, J. P. M.; van Gunsteren, W. F.; DiNola, A.; Haak, J. R. *J. Chem. Phys.* **1984**, *81*, 3684.

(21) Hess, B.; Bekker, H.; Berendsen, H. J. C.; Fraaije, J. G. E. M. *J. Comput. Chem.* **1997**, *18*, 1463.

(22) Miyamoto, S.; Kollman, P. A. *J. Comput. Chem.* **1992**, *13*, 952.

(23) Feenstra, K. A.; Hess, B.; Berendsen, H. J. C. *J. Comput. Chem.* **1999**, *20*, 786.

(24) Bogusz, S.; Venable, R.; Pastor, R. *J. Phys. Chem. B*, in press.